# Origin of Plasticity Length-Scale Effects in Fracture

Srinath S. Chakravarthy and William A. Curtin

*Division of Engineering, Brown University, Providence, Rhode Island 02912, USA*

(Received 26 May 2010; published 7 September 2010)

Fracture in metals is controlled by material behavior around the crack tip where size-dependent plasticity, now widely demonstrated at the micron scale, should play a key role. Here, a physical origin of the controlling length scales in fracture is identified using discrete-dislocation plasticity simulations. Results clearly demonstrate that the spacing between obstacles to dislocation motion controls fracture toughness. The simulations support a continuum strain-gradient plasticity model and provide a physical interpretation for that model's phenomenological length scale. Analysis of a dislocation pileup under a stress gradient predicts the yield stress to increase with increasing obstacle spacing, physically rationalizing the simulations.

DOI: 10.1103/PhysRevLett.105.115502 PACS numbers: 62.20.mm

Engineering design of essentially all metallic components used in structural applications, aircraft structures, cars, bridges, pacemakers, hip implants, computer chip packages, turbine disks, among others—relies heavily on the long-standing framework of continuum plasticity. However, many experiments now show that the plastic flow stress in metals increases in material volumes on the micron scale and below [1–7]. Micro- and nanoindentation hardness of metals [1,2], the flow strength of nanocrystalline metals [3,4], nano- and micropillar [5], nanoasperities [6], and thin films [7], all obey the mantra of ''smaller is stronger'' and highlight the failure of conventional continuum plasticity. The region around a crack tip is a micron-scale material volume that arises in all larger-scale structures. In many cases continuum plasticity does not predict growth of an initial crack, whereas cracks do grow in real materials [8]. These issues have spurred new approaches to plasticity such as phenomenological strain-gradient plasticity (SGP) models [9–12] and discrete-dislocation models [13–15]. However, no clear physical identification of material length scales controlling size dependence exists, in spite of wide speculation on possible length scales [16]. Here, we use a new discrete-dislocation (cohesive-zone) model to unambiguously demonstrate that the spacing between obstacles to dislocation motion is one dominant material length scale controlling the fracture toughness of plastically deforming metals. Our results support one SGP model [17] and provide a physical interpretation for that model's phenomenological length scale. We then show that the behavior of dislocations in a ''pileup'' at an obstacle under a stress gradient rationalizes our results and points in a new direction for understanding some size effects in plasticity.

The generic discrete-dislocation (DD) [cohesive-zone (CZ)] methodology is described in the recent literature [18–20]. Briefly, the method used here treats edge dislocations as line defects with Burgers vector $b$, in a plane-strain elastically isotropic (shear modulus $\mu$, Poisson's ratio $\nu$) single-crystal material with 3 slip systems oriented at 60° relative to one another and parallel slip planes spaced by $100b$. To gain quantitative control over the material description and to model fracture for realistic material parameters requires new insights and new algorithms. One key feature of our DD formulation is that the motion of dislocations along their slip planes is impeded by obstacles of strength $\tau_{\rm obs}$ having average spacing $L_{\rm obs}$, with each ''obstacle'' physically representing an array of obstacles in the third dimension [21]. We have recently shown that the macroscopic plastic flow is controlled by dislocation pileups at the obstacles so that the uniaxial tensile yield stress is given by [21]

$$\sigma_Y = \frac{1}{S}\sqrt{\frac{4\mu b}{\pi(1-\nu)}\frac{\tau_{\rm obs}}{1.5L_{\rm obs}} + \tau_s^2}, \tag{1}$$

where $S$ is the Schmid factor. This obstacle-controlled material model corresponds most closely to precipitation-hardened materials with high strength and low strain hardening rates, such as the commercially important Al-2$XXX$, Al6$XXX$, Al-7$XXX$ alloys and radiation-hardened metals. One such material is Al-2024 (Al-Cu-Mg) which, as a function of aging, has yield strengths in the range of 350–500 MPa, low hardening exponents (0.05–0.15), and shows size effects that have been interpreted within an SGP model to have gradient length parameters of 50–200 nm [22] that are comparable to the operative lengths in our study. Of most importance, Eq. (1) shows that the macroscopic yield stress $\sigma_Y$ can be held fixed while the internal length scale and obstacle strength can be varied, permitting control of the material length scale $L_{\rm obs}$.

To model fracture, we insert an initial crack into the material described above and introduce a cohesive-zone model along the crack line. A far-field mode-I stress intensity load is applied and crack growth occurs naturally when conditions near the crack allow the cohesive zone to open. A schematic of the fracture test is shown in Fig. 1.

 

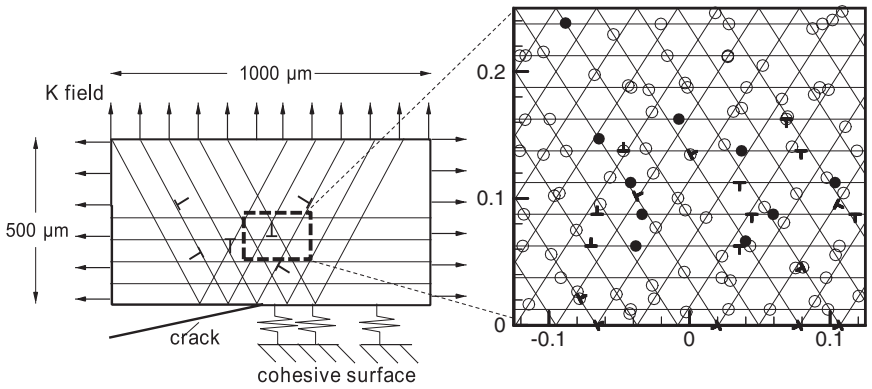


FIG. 1. Schematic of the top half of the symmetric DD[CZ] fracture simulation geometry. A remote stress intensity loading is applied to a material that deforms via dislocation plasticity and that contains an initial crack and cohesive zone along the line ahead of the crack. The nanoscale material model consists of dislocations, dislocation slip planes, dislocation sources (solid circles), and dislocation obstacles (open circles). Lengths are in microns.

The primary properties of any cohesive zone are the cohesive strength $\sigma_{\rm coh}$, typically 2–20 GPa, and the fracture energy $\Gamma_0$, typically a few J/m$^2$. Continuum plasticity models predict no crack growth in the regime $\sigma_{\rm coh}/\sigma_Y >$ 3–5 [23] which is typically exceeded in most realistic materials and has thus driven the application of SGP or DD treatments of the plasticity. Two characteristic lengths associated with the cohesive zone are the critical opening $\sim\Gamma_0/\sigma_{\rm coh}$, typically 0.1 nm and thus comparable to the dislocation Burgers vector, and the critical cohesive length, $\sim\mu\Gamma_0/\sigma_{\rm coh}^2$, typically 1 nm. Resolving the stress and strain fields over the nanometer scale, capturing the interaction of dislocations with a nanoscale cohesive zone, and modeling crack growth over the several microns needed to establish the material fracture toughness, all represent significant numerical challenges that we have overcome by a host of new algorithms to be reported elsewhere. Here, we fix the material parameters as $\Gamma_0 = 1.1$ J/m$^2$, $\sigma_{\rm coh} = 7$ GPa, $\mu = 63.9$ GPa, $\nu = 0.33$, and $b = 0.25$ nm to match the values used in a recent SGP model of fracture [17]. Then, for any fixed yield stress $\sigma_Y$, we vary the obstacle spacing $L_{\rm obs}$ between 62.5 and 250 nm, and vary $\tau_{\rm obs}$ accordingly. Varying $\sigma_Y$ is achieved by changing $\tau_{\rm obs}$ with all other parameters fixed. The yield stresses used here (600–800 MPa) are somewhat higher than the Al-*XXXX* materials of practical interest so as to make the study computationally feasible and to make contact with SGP modeling.

The inset in Fig. 2 shows one example of the evolution of the applied loading as a crack grows. Growth begins around the elastic limit $\Gamma_0$ but dislocation generation and motion dissipate energy and stabilize the crack so that increasing load is required to drive the crack further. At a critical load that defines the fracture energy $\Gamma_c$, the plastic response of the material cannot prevent crack growth and the crack grows with no further increase in load. Figure 2 shows that, for several values of yield stress, the normalized fracture energy $\Gamma_c/\Gamma_0$ increases with decreasing obstacle spacing $L_{\rm obs}$ with all other material and computational parameters held fixed. We can thus unambiguously identify the obstacle spacing $L_{\rm obs}$ as the physical material length scale that controls fracture toughness; this is the main result of this Letter.

Figure 2 also shows the predicted fracture energy using the Fleck-Hutchinson (FH) SGP model [23] for fracture along a bimaterial metal-ceramic interface [17] using the same CZ model parameters and $\sigma_Y = 700$ MPa. The SGP length parameter $L_{\rm FH}$ has been scaled to best match the simulation data; excellent agreement is obtained for $L_{\rm FH} \sim \frac{1}{5}L_{\rm obs}$. The SGP model predicts that the toughness depends only on the ratio $\sigma_{\rm coh}/\sigma_Y$, and so Fig. 2 also compares SGP predictions for $\sigma_Y/\sigma_{\rm coh} = 11.86$ at $\sigma_Y = 700$ MPa to our simulations at $\sigma_{\rm coh}/\sigma_Y = 11.66$ and $\sigma_Y = 600$ MPa; agreement is again good. Capturing the simulation trend with both material length scale and yield stress is a strong validation of this SGP model. The correspondence between our DD simulation, where the size effects in fracture arise as a natural outcome of dislocation physics, and a phenomenological continuum SGP model is the second main result of this Letter.

We now provide more physical insight into the dependence of the fracture toughness on obstacle spacing. Since the yield stress is controlled by dislocation pileups at obstacles [Eq. (1)], we analyze the behavior of pileups in the presence of a stress gradient. Using a continuously distributed dislocation density $n(x)$ in the range $-\frac{1}{2}L_{\rm obs} < x < \frac{1}{2}L_{\rm obs}$ between two obstacles, and, for simplicity, zero source strength $\tau_s = 0$ at $x = 0$, the equilibrium pileup density satisfies [24]

$$\tau_{\rm app}(x)b + \frac{\mu b^2}{2\pi(1-\nu)}\int\frac{n(x')}{x-x'}dx' = 0, \qquad -\frac{L_{\rm obs}}{2} \le x \le \frac{L_{\rm obs}}{2}. \quad (2)$$

When the applied stress varies linearly, $\tau_{\rm app}(x) = \tau_{\rm app}(1 - \chi x)$, with $\tau_{\rm app}\chi$ the magnitude of the stress gradient,

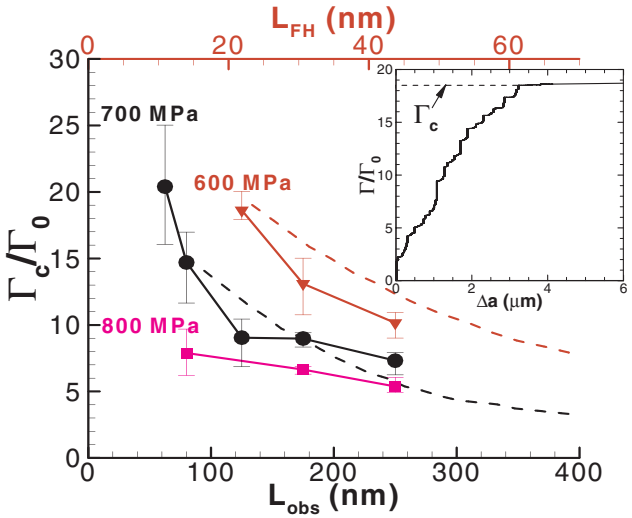


FIG. 2 (color online). Normalized fracture energy $\Gamma_c/\Gamma_0$ versus dislocation obstacle spacing $L_{\text{obs}}$, for various values of the tensile yield stress. Error bars show variations using three statistically different realizations of dislocation obstacles and sources in the simulation. Dashed lines: predictions of SGP theory [17] with gradient length scaled to match simulations (upper scale). Inset: growth of fracture toughness with crack growth, due to evolution of dislocation plasticity, for one particular sample ($L_{\text{obs}} = 80$ nm, $\sigma_Y = 700$ MPa).

Eq. (2) can be solved analytically for $n(x)$. The yield stress $\sigma_Y'$ is the applied tensile stress ($\sigma_{\text{app}} = \tau_{\text{app}}/S$) at which the dislocation at both obstacles attain or exceed the obstacle strength, a condition used to obtain Eq. (1) [21]. Denoting the tensile yield stress with zero gradient as $\sigma_Y$, the yield stress $\sigma_Y'$ in the stress gradient is

$$\sigma_Y' = \frac{\sigma_Y}{(1-0.5\chi L_{\text{obs}})}. \quad (3)$$

For fixed gradient $\chi$, Eq. (3) predicts an increase in the yield stress with increasing $L_{\text{obs}}$. The concept of "stress gradient plasticity" embodied in Eq. (3) has broad implications for size-dependent plasticity that will be explored separately. Applied to fracture, Eq. (3) predicts that, since the stress gradient near the crack tip is larger than farther away, the near-tip yield stress $\sigma_Y'$ controlling fracture is larger than the nominal yield stress $\sigma_Y$ and increases with increasing $L_{\text{obs}}$. Since fracture toughness decreases with increasing yield stress (Fig. 2), higher $\sigma_Y'$ leads to lower fracture toughness with increasing $L_{\text{obs}}$, consistent with Fig. 2. Figure 3 shows an averaged measure of the local plastic strain around the crack tip in two simulations at the same applied load level and same yield stress $\sigma_Y$ but with different $L_{\text{obs}}$. There is considerably less slip in the material with larger $L_{\text{obs}}$, consistent with the model prediction of a higher yield stress $\sigma_Y'$. Quantitatively, if we linearize the crack tip elastic field around the nearest typical dislocation source at $x_0 = \rho_s^{-1/2} = 150$ nm away from the crack tip, we obtain $\chi = 0.5/x_0$. Figure 4 shows that the fracture toughness $\Gamma_c/\Gamma_0$ versus $\sigma_{\text{coh}}/\sigma_Y'$ then collapses onto a single curve. The lower toughness for materials with larger $L_{\text{obs}}$ is thus partially a reflection of the decreasing value of $\sigma_{\text{coh}}/\sigma_Y'$. The importance of stress gradients near the crack tip in controlling the size-dependent material flow and fracture is the third main result of this Letter.

Some limitations of the DD method exist, such as the restriction to plane-strain edge dislocations, no crack tip dislocation nucleation and associated crack tip blunting, and the absence of fully $3d$ mechanisms of hardening. However, none of these features are explicitly contained within the continuum SGP models either. We also note

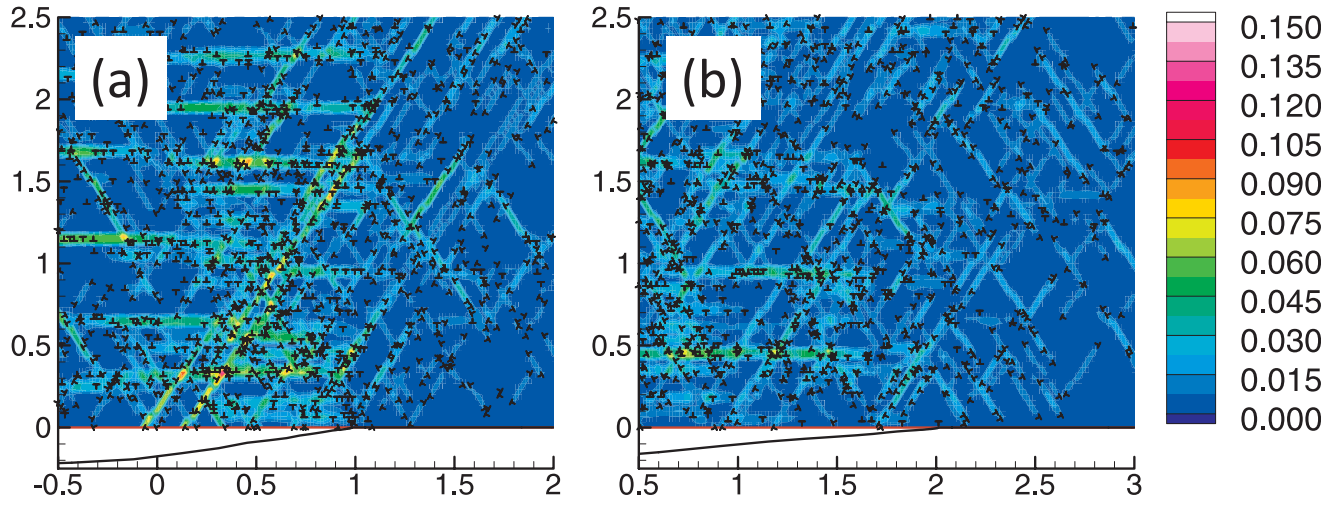


FIG. 3 (color). Contours of averaged local plastic strain from DD simulations and crack opening profile (curves, displacement ×10) for materials with (a) $L_{\text{obs}} = 80$ nm and (b) $L_{\text{obs}} = 250$ nm, at the same load $\Gamma/\Gamma_0 = 5.25$ and tensile yield stress $\sigma_Y = 700$ MPa. Actual dislocations are shown as symbols, and the dislocation densities in the region shown are (a) $2 \times 10^{14}/\text{m}^2$ and (b) $1 \times 10^{14}/\text{m}^2$. All lengths are in microns.

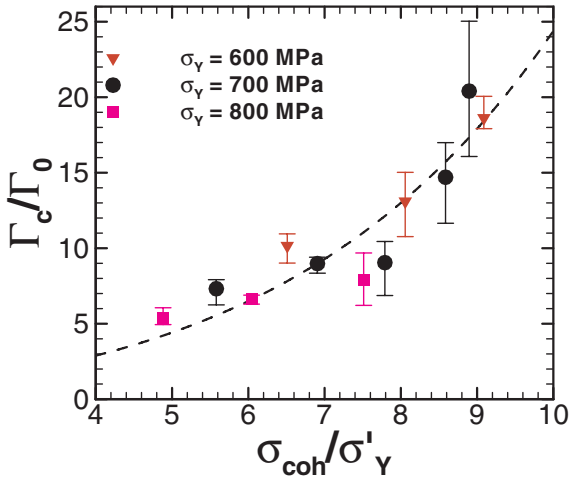


FIG. 4 (color online). Fracture toughness versus $\sigma_{\mathrm{coh}}/\sigma_Y'$ where $\sigma_Y'$ is the near-crack-tip yield stress [see Eq. (3)], which approximately collapses data from Fig. 2 onto a single curve (dashed line to guide the eye).

that, for the precipitation-hardened materials to which our material model is most applicable, $3d$ hardening effects play a lesser role than in other materials such as pure metals. Incorporating the features above is possible [25,26] but with greatly increasing computational effort. With these caveats, our results nonetheless show that DD simulations are an effective computational laboratory for guiding interpretation of SGP models.

In summary, a number of candidate material length scales have been proposed as sources of size effects in plasticity but no clear quantifiable evidence has emerged from either experiment or prior theory. The DD virtual laboratory allows for independent variation of internal material parameters, control that is absent in continuum theories and difficult to attain via experiments. Applied to fracture, the model has revealed one definite, physical, material length scale controlling fracture toughness in metals and a simple analytic model aids in understanding how this length scale operates to increase the material flow stress near the crack tip, driving fracture.

The authors gratefully acknowledge support from NASA Langley Research Center (Grant No. NNX07AU56A) and the NSF Materials Research Science and Engineering Center at Brown on "Micro- and Nano-mechanics of Materials" (DMR-0520651).

[1] Q. Ma and D. R. Clarke, J. Mater. Res. **10**, 853 (1995).
[2] N. Stelmashenko, M. Walls, L. Brown, and Y. Milman, Acta Metall. Mater. **41**, 2855 (1993).
[3] K. Lu, L. Lu, and S. Suresh, Science **324**, 349 (2009).
[4] S. Yip, Nature Mater. **3**, 11 (2004).
[5] M. D. Uchic, D. M. Dimiduk, J. N. Florando, and W. D. Nix, Science **305**, 986 (2004).
[6] D. K. Ward, D. Farkas, J. Lian, W. A. Curtin, J. Wang, K. Kim, and Y. Qi, Proc. Natl. Acad. Sci. U.S.A. **106**, 9580 (2009).
[7] R. Venkatraman and J. Bravman, J. Mater. Res. **7**, 2040 (1992).
[8] D. Korn, G. Elssner, R. M. Cannon, and M. R'ühle, Acta Mater. **50**, 3881 (2002).
[9] W. D. Nix and H. Gao, J. Mech. Phys. Solids **46**, 411 (1998).
[10] N. A. Fleck and J. W. Hutchinson, Adv. Appl. Mech. **33**, 295 (1997).
[11] A. Acharya and J. L. Bassani, J. Mech. Phys. Solids **48**, 1565 (2000).
[12] M. E. Gurtin, J. Mech. Phys. Solids **48**, 989 (2000).
[13] B. Devincre, T. Hoc, and L. Kubin, Science **320**, 1745 (2008).
[14] R. Madec, B. Devincre, L. Kubin, T. Hoc, and D. Rodney, Science **301**, 1879 (2003).
[15] E. Van der Giessen and A. Needleman, Model. Simul. Mater. Sci. Eng. **3**, 689 (1995).
[16] A. Evans and J. Hutchinson, Acta Mater. **57**, 1675 (2009).
[17] Y. Wei and J. W. Hutchinson, Philos. Mag. **88**, 3841 (2008).
[18] M. O'Day and W. Curtin, J. Mech. Phys. Solids **53**, 359 (2005).
[19] V. S. Deshpande, A. Needleman, and E. Van der Giessen, Acta Mater. **51**, 1 (2003).
[20] N. Broedling, A. Hartmaier, and H. Gao, Int. J. Fract. **140**, 169 (2006).
[21] S. Chakarvarthy and W. Curtin, J. Mech. Phys. Solids **58**, 625 (2010).
[22] Y. Ro, M. Begley, R. Gangloff, and S. Agnew, Mater. Sci. Eng. A **435–436**, 333 (2006).
[23] Y. Wei and J. W. Hutchinson, J. Mech. Phys. Solids **45**, 1253 (1997).
[24] J. P. Hirth and J. Lothe, *Theory of Dislocations* (Wiley, New York, 1982), 2nd ed.
[25] V. S. Deshpande, A. Needleman, and E. Van der Giessen, J. Mech. Phys. Solids **51**, 2057 (2003).
[26] A. A. Benzerga, Y. Bréchet, A. Needleman, and E. Van der Giessen, Model. Simul. Mater. Sci. Eng. **12**, 159 (2004).